Synthesis, linear extinction, and preliminary resonant hyper-Rayleigh scattering studies of gold-core/silver-shell nanoparticles: comparisons of theory and experiment

Youngjin Kim, Robert C. Johnson, Jiangtian Li, Joseph T. Hupp [*],
George C. Schatz [1]

*Department of Chemistry, Materials Research Center and Center for Nanofabrication and Molecular Self-Assembly,
Northwestern University, 2145 Sheridan Road, Evanston, IL 60208-3113, USA*

Abstract

Gold-core/silver-shell nanoparticles featuring core diameters of 13 or 25 nm were prepared in aqueous solution. Silver-coated gold nanoparticles have two distinct plasmon absorption bands whose relative intensities depend on the shell thickness – features that are captured well by classical Mie theory. The core/shell spectra are not simply linear combinations of the pure-component spectra. Theory shows that shell dielectric effects upon the core can cause broadening, shifting, and, in some cases, damping of dominant extinction spectral features. Preliminary studies show that core–shell particles are reasonably efficient hyper-Rayleigh scatterers under conditions of two-photon resonance or near resonance with a high-energy plasmon band. © 2002 Published by Elsevier Science B.V.

1. Introduction

Nanoscale metal particles have attracted significant recent attention because of their unusual size-dependent optical and electronic properties and because of their potential for application in novel electronic devices, nonlinear optical devices, chemical and biochemical sensors, and catalysis [1–10]. Nanoparticles of free-electron metals, especially silver, gold, and copper, have been of particular interest spectroscopically because of their intense visible-region extinction – a property largely due to surface plasmon absorption (collective excitation of conduction-band electrons) [11]. The intense absorption and accompanying excitation translate into greatly enhanced local electromagnetic fields – which in turn can enhance otherwise weak multi-photon processes such as Raman scattering [12–15] and hyper-Rayleigh scattering (HRS) [8,16–20].

We have begun investigating metal-core/metal-shell particles from the point of view of optimizing 'hyper-photonic' behavior, especially HRS. We note that the γ-irradiation based preparation, and

---

[*] Corresponding author. Fax: +1-847-491-7713.

E-mail addresses: jthupp@chem.nwu.edu (J.T. Hupp), schatz@chem.nwu.edu (G.C. Schatz).

[1] Also corresponding author.

linear optical characterization, of Ag/Cd, Ag/Pb, and Ag/In core/shell particles was reported as early as 1980 by Henglein and co-workers [21,22]. More recently, Henglein has described the preparation and linear optical characterization of Au/Pt and Pt/Au core/shell particles [23]. More closely related to the work described here are reports by Mulvaney et al. [24], and by Kreibig and co-workers [25], on the preparation and linear optical characterization of particles featuring 6 nm diameter Ag cores and Au shells of varying thickness, and by Link et al. [26] on 17–25 nm diameter Au–Ag alloy nanoparticles. Both groups reported deviations in optical behavior from the simplest expectations of classical Mie theory [27,28]. In Mulvaney's work, the case was convincingly made that the deviations were due to significant alloy formation. In Link's study, agreement was obtained once experimentally determined alloy dielectric constants were substituted for simple composition-weighted averages in the Mie treatment.

Here we report the synthesis and linear optical properties of gold-core/silver-shell nanoparticles ranging in diameter from about 14 to about 27 nm. We find that the particles' linear extinction spectra are reasonably well described by Mie theory over the range of core and shell sizes examined. We also report on preliminary studies of HRS for particles featuring 13 nm gold cores and various sized silver shells, under conditions of two-photon resonance or near resonance with a high-energy plasmon band.

2. Experimental

2.1. Reagents

HAuCl$_4$ (Aldrich Chemical), silver nitrate (Mallinckrodt), and citric acid trisodium salt (J.T. Baker Chemical) were used as received. Distilled water was purified with a Quantum EX Millipore system (> 18 MΩ) and passed through a 0.22 μm particulate filter.

2.2. Preparation of colloidal nanoparticles

Colloidal Au particles (13 and 25 nm diameter) were prepared by citrate reduction of HAuCl$_4$ as reported previously [29,30]. Gold-core/silver-shell nanoparticles were prepared by using a 'seed colloid' technique [31] as follows. An aqueous AgNO$_3$ solution was added to a boiling solution of 13 or 25 nm gold particles (0.91 mM based on atoms), followed by 0.86 ml of 1.0% sodium citrate solution. Heating was continued for 1 h followed by slow cooling to room temperature. In the modified procedure, the silver shell thickness is controlled by varying the amount of AgNO$_3$ solution added to the bare gold particles. Core/shell particles with nominal silver mole fractions, χ_{Ag}, of 0.14, 0.25, 0.40, 0.50, and 0.57, and gold core diameters of 13 and 25 nm were prepared in this way.

2.3. Measurements

UV–visible extinction spectra were recorded with a HP 8524A diode array spectrophotometer. Particle sizes were evaluated by high-resolution transmission microscopy (HRTEM) using a Hitachi HF-2000 filed emission TEM operating at 200 kV. From the TEM images the size distributions of the samples are determined by counting at least 280 particles. Elemental analysis (Au and Ag) in the core–shell particles was determined by inductively coupled plasma (ICP, ATOMSCAN 25 spectrometer) measurements. HRS measurements of colloidal suspensions of core/shell particles were performed by using a mode-locked Ti:sapphire laser source and lock-in detection as previously described [17,18]. Nanoparticle HRS intensities were calibrated by using HRS from the solvent (water) as an internal reference [8].

3. Results and discussion

3.1. Nanoparticle synthesis

Fig. 1 shows TEM-derived histograms of particle size for a nominally 25 nm diameter gold nanoparticle sample and for a sample that had been further reacted with AgNO$_3$ to create a silver shell. The histograms show that: (a) reasonably low size-polydispersity is obtained, and (b) the core/shell particles are, on average, larger than the parent
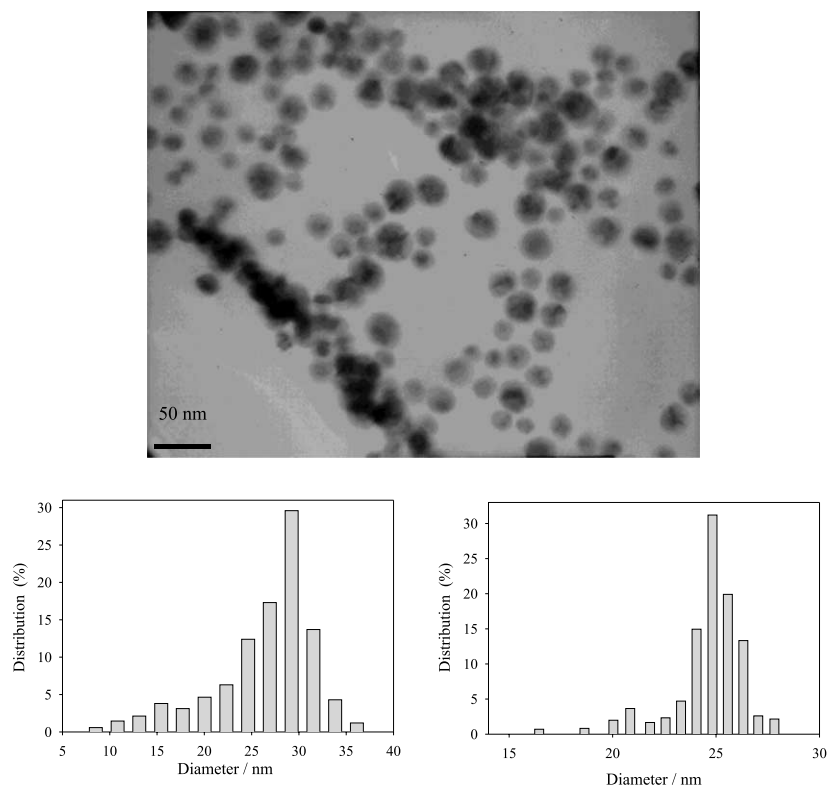
Fig. 1. TEM image of 25 nm gold particles coated with 4 nm of silver. This corresponds to a silver mole fraction of 0.56. Bottom left: particle size histogram for this colloid derived from TEM data. Bottom right: histogram for a parent gold-core particle sample.

core particles. For the example shown, the average radii are 24.8 ± 1.5 nm and 29.2 ± 2.3 nm, as determined by computer-based measurement of the particle diameters. It is clear that the observed dimensional changes are consistent with those expected based on quantitative conversion of added silver ions to silver-shell material. It is also clear, however, that the uncertainties in the measurements are large enough that particle size changes associated with shell formation cannot be used to establish with reliability the overall elemental composition. ICP measurements of elemental composition were made for three representative Au core/Ag shell particle samples and are consistent with the expected compositions assuming quantitative reaction of starting materials. (For samples with 13 nm cores: χ_{Ag}(expected) $= 0.14$, χ_{Ag} (observed) $= 0.14 \pm 0.01$; χ_{Ag}(expected) $= 0.38$, χ_{Ag}(observed) $= 0.40 \pm 0.02$. For a sample with a

25 nm core: χ_{Ag}(expected) $= 0.47$, χ_{Ag} (observed) $= 0.50 \pm 0.03$).

3.2. Linear extinction spectra

Measured spectra of Au-core/Ag-shell particles featuring 13 and 25 nm core diameters are shown in Fig. 2. The spectra are scaled such that each describes the same total number of gold atoms, i.e., the 'molar' units for extinction coefficients are referenced to the concentration of gold atoms, not total metal atoms, present. Shown for comparison in Fig. 2 are extinction spectra for 13 and 25 nm particles of pure gold. Particles of pure silver of similar sizes display a sharp, very intense plasmon absorption peak centered at 390–400 nm.

Clearly evident, especially at low silver concentrations, is the presence of two absorption bands at energies close to those of the plasmon
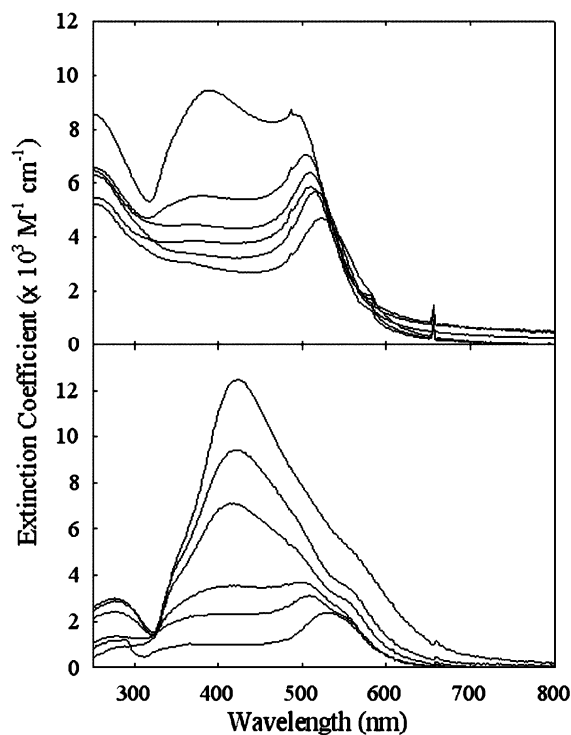
Fig. 2. Measured extinction spectra of 13 nm (top) and 25 nm (bottom) gold particles with silver shells corresponding to silver mole fractions of 0, 0.14, 0.25, 0.40, 0.50, and 0.57, with the lowest extinction curve in each panel corresponding to pure gold particles. The units for extinction are based on moles of metal atoms, not moles of particles.
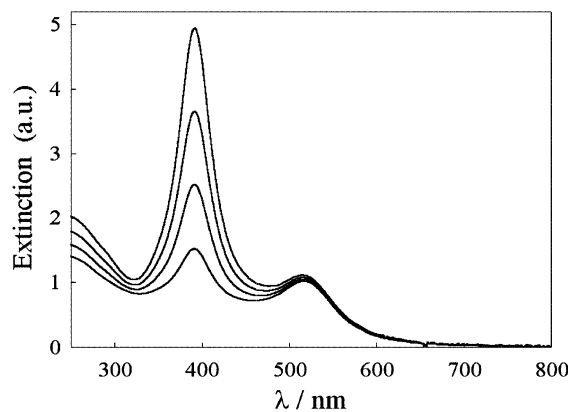

Fig. 3. Linear combinations of extinction spectra of 13 nm gold particles and 10 nm silver particles. The combined spectra feature a fixed amount of gold, with added silver yielding silver mole fractions of 0.20, 0.35, 0.46, and 0.55. In a core/shell geometry, these mole fractions would correspond to silver shell thicknesses of 0.5, 1.0, 1.5, and 2.0 nm based on a 13 nm gold core.

absorption bands of the parent compounds. This implies that alloy formation does not dominate the putative core/shell nanoparticle synthesis process – a single band at intermediate energies being expected for particles that have alloyed. While not inconsistent with theory (see below), also striking is the presence of a well-defined plasmon band for silver under conditions where the average shell thickness is as little as ca. 0.6 nm. (Note that an isolated cluster of silver atoms ca. 0.6 nm in diameter would consist of only about 10 atoms and would not display plasmon absorption.)

With increasing silver content, the plasmon band of gold for each series of core/shell particles shifts toward shorter wavelengths, eventually being damped by the shell and hidden by the intense silver plasmon band. At the same time, the silver plasmon band shifts to longer wavelengths for progressively thicker shells. That the observed spectra for core/shell particles are not simply linear combinations of spectral properties for the component metals is shown in Fig. 3 where artificial spectra of this kind have been constructed.

3.3. Spectral simulations: model

It is well established that the optical absorption spectra of free-electron metal nanoparticles, such as Ag and Au, consist of strong bands that originate from plasmon excitations. Therefore, we would also expect the optical spectra of metal nanoshells to be plasmonic in origin. Mie theory explains the linear extinction spectra of spherical nanoparticles of free-electron metals using classical electrodynamics. We employ a generalized Mie expression to calculate the combined absorption and scattering cross-sections of Au-core/Ag-shell nanoparticles. For a homogeneous sphere, this extinction cross-section is given by

$$C_{\text{ext}} = \frac{2\pi}{k^2} \sum_{n=1}^{\infty} (2n+1)Re\{a_n + b_n\}, \tag{1}$$

where the scattering coefficients are given by:

$$a_n = \frac{m\psi_n(mx)\psi_n'(x) - \psi_n(x)\psi_n'(mx)}{m\psi_n(mx)\xi_n'(x) - \xi_n(x)\psi_n'(mx)} \qquad (2)$$

and

$$b_n = \frac{\psi_n(mx)\psi_n'(x) - m\psi_n(x)\psi_n'(mx)}{\psi_n(mx)\xi_n'(x) - m\xi_n(x)\psi_n'(mx)}. \qquad (3)$$

In Eqs. (2) and (3), $\psi_n(\rho)$ and $\xi_n(\rho)$ are Riccati–Bessel functions; x is a size parameter equal to $2\pi Na/\lambda$ where a is the radius of the sphere; and m equals N_1/N, the ratio of the refractive indices of the particle and medium, respectively.

For a spherical core having a homogeneous shell of uniform thickness, application of electromagnetic boundary conditions at both the inner and outer shell surfaces gives expressions for the coefficients a_n and b_n as follows:

$$
\begin{aligned}
a_n = &\Big\{ \psi_n(y)[\psi_n'(m_2 y) - A_n\chi_n'(m_2 y)] \\
&- m_2\psi_n'(y)[\psi_n(m_2 y) - A_n\chi_n(m_2 y)] \Big\} \\
&\Big/ \Big\{ \xi_n(y)[\psi_n'(m_2 y) - A_n\chi_n'(m_2 y)] \\
&- m_2\xi_n'(y)[\psi_n(m_2 y) - A_n\chi_n(m_2 y)] \Big\} \qquad (4)
\end{aligned}
$$

and

$$
\begin{aligned}
b_n = &\Big\{ m_2\psi_n(y)[\psi_n'(m_2 y) - B_n\chi_n'(m_2 y)] \\
&- \psi_n'(y)[\psi_n(m_2 y) - B_n\chi_n(m_2 y)] \Big\} \\
&\Big/ \Big\{ m_2\xi_n(y)[\psi_n'(m_2 y) - B_n\chi_n'(m_2 y)] \\
&- \xi_n'(y)[\psi_n(m_2 y) - B_n\chi_n(m_2 y)] \Big\}, \qquad (5)
\end{aligned}
$$

where

$$A_n = \frac{m_2\psi_n(m_2 x)\psi_n'(m_1 x) - m_1\psi_n'(m_2 x)\psi_n(m_1 x)}{m_2\chi_n(m_2 x)\psi_n'(m_1 x) - m_1\chi_n'(m_2 x)\psi_n(m_1 x)} \qquad (6)$$

and

$$B_n = \frac{m_2\psi_n(m_1 x)\psi_n'(m_2 x) - m_1\psi_n(m_2 x)\psi_n'(m_1 x)}{m_2\chi_n'(m_2 x)\psi_n(m_1 x) - m_1\psi_n'(m_1 x)\chi_n(m_2 x)}. \qquad (7)$$

In these equations, the subscripts 1 and 2 refer to the core and shell, respectively; a and b are the inner and outer radii of the coated sphere; and $\chi_n(\rho)$ is the Riccati–Bessel function that corresponds to the y_n Bessel function.

For a complete description of the plasmon absorption of core/shell particles, absorption band broadening mechanisms must be considered. When the particle size is smaller than the conduction electron mean free path, the metal dielectric constant changes because electrons scatter from the particle surfaces [28]. Literature values for the dielectric constants of gold and silver [32] were modified by adding a correction to the bulk plasmon width involving the Fermi velocity divided by an effective length [33]. For the core, this length was equated with the core radius (which is the average classical pathlength in a sphere [33]); for the shell, it was equated with the shell thickness. This assumes that the conduction electrons scatter incoherently at the Au/Ag interface as well as at the outer surface of the particle. Similar calculations performed without applying this size-dependent correction yielded extinction spectra with notably poorer agreement with the experimental spectra. The most obvious change upon elimination of the correction is a sharpening and intensification of the higher-energy silver-like plasmon absorption band. Still, it should be noted that a definitive statement about the accuracy of either method is difficult to make, since structural defects and particle inhomogeneities that are not taken into account in the Mie calculations are likely to affect the extinction spectra.

3.4. Spectral simulations: data

Fig. 4 shows calculated nanoparticle extinction spectra for the full range of core and shell sizes examined. Briefly, the calculations reproduce the dominant features of the experimental spectra, including: (a) the appearance of two plasmon bands for nanoparticles possessing thin or only moderately thick shells, (b) systematic blue shifts and intensity damping for the gold-core plasmon absorption with increasing shell thickness, and (c) systematic red shifts in silver plasmon absorption with increasing shell thickness. That agreement with experiment is not perfect may well reflect particle size dispersion, shell non-uniformity, and departures from perfectly spherical particle geometries in the experimental samples.
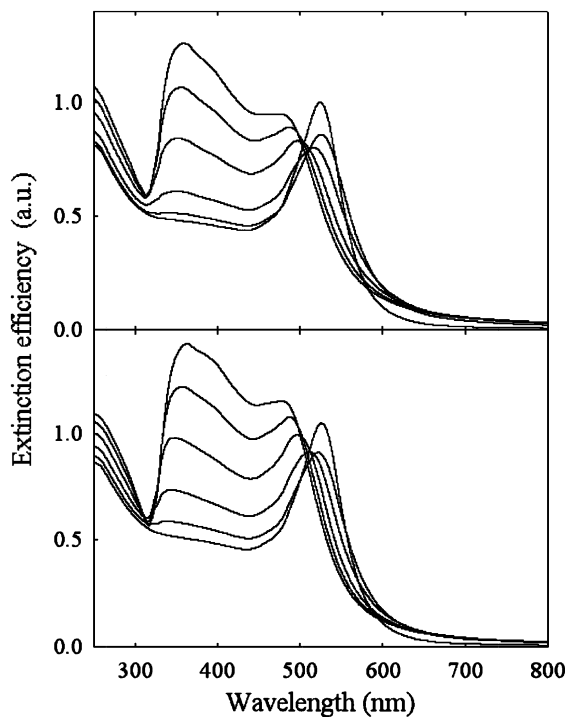
Fig. 4. Calculated extinction spectra of gold core/silver shell particles with the same compositions and dimensions as those shown in Fig. 2.

Both experiment and theory yield silver plasmon bands that, particularly in the thick shell limit, are broader than the observed with pure silver nanoparticles of similar size. The broadening likely arises from both the limited shell thickness, which shortens the electron mean-free path as noted above, and the presence of a high-dielectric core, which modifies scattering coefficients in a complex way (cf. Eqs. (4) and (5) vs. (2) and (3)). The presence of a high-dielectric shell, on the other hand, predictably damps the intensity of the plasmon absorption of the gold core. (Note that the solvent (water) also damps the plasmon intensity, but the higher dielectric and more proximal silver shell does so more effectively – and increasingly so, as the shell thickness increases.)

Finally, while the spectra calculated for fixed ratios of core diameter to shell thickness are remarkably similar for particles of differing overall size, the largest particles consistently display broader plasmon features than do smaller particles. The difference could reflect a greater role for the quadrupole moment for the largest particles, as well as greater radiative damping. The most important contributor to the broadening, however, is probably particle size or shape inhomogeneity. For example, since deposition of the shell material should occur faster on larger core particles, a slight degree of polydispersity in the core particle size distribution could be magnified upon core–shell particle formation, yielding broadened plasmon peaks.

3.5. Hyper-Rayleigh scattering

A preliminary study of HRS by particles featuring 13 nm cores and silver shells of various thicknesses was undertaken. HRS from gold nanoparticles is extremely efficient and is known to be significantly enhanced due to plasmon resonance effects. We reasoned that gold-core/silver-shell particles might show especially strong HRS if examined under conditions of resonance with the high-energy silver-like plasmon band. Because light-absorbing colloidal metal nanoparticles are subject to photo damage, we chose to excite the particles off-resonance, with the resonance instead being achieved with the exciting frequency-doubled photons. Fig. 5 shows the HRS response at 410 nm from core/shell particle suspensions in water at three different particle concentrations, based on excitation at 820 nm. The responses show the expected scaling of HRS intensity with the square of the power of the incident light. The inset shows that the signal is nearly monochromatic and centered at 410 nm, confirming the assignment as HRS and ruling out an alternative assignment as two-photon-absorption-induced fluorescence. Returning to the central portion of the figure, the HRS intensity is observed to scale linearly with the nanoparticle concentration, thereby ruling out the possibility of significant contributions due to residual coherent second harmonic generation. (Neglecting absorption losses, the intensity for coherent frequency doubling should scale as the square of the particle concentration. HRS can be viewed essentially as incoherent SHG, where the lack of coherence reflects the fact that the particle and interface sizes
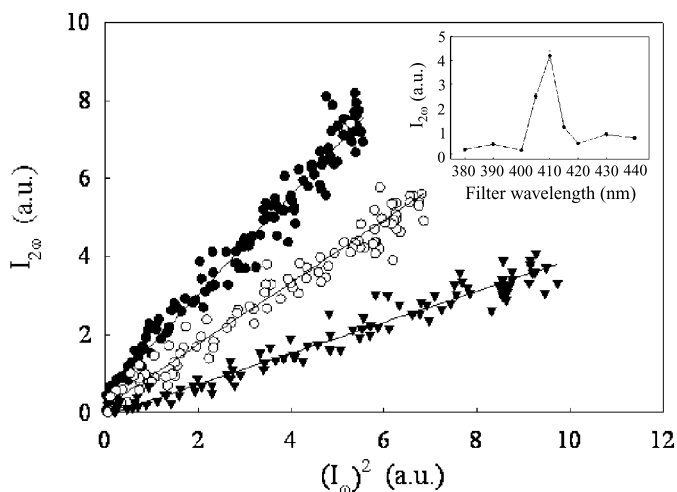
Fig. 5. Dependence of hyper-Rayleigh scattering intensity, $I(2\omega)$, on incident intensity squared, $I^2(\omega)$, for various concentrations of 13 nm gold core/silver shell particles (silver mole fraction is 0.50). Inset shows that the observed signal is monochromatic.

are small compared with the wavelengths of incident and doubled light.)

Quantitative analyses of two-photon scattering efficiencies are possible based on comparisons of the HRS response to the response from the solvent itself [8]. Because signals scale with the square of the first hyperpolarizability, β, and because different sets of particles have different volumes and different numbers of atoms, the best figure of merit likely is β^2/atom. To facilitate comparisons with other hyper-photonic chromophores, it is useful to define further a quantity, β' $(= [\beta^2/\text{atom}]^{1/2})$ [18,19]. For 13 nm gold particles prepared as described here, we typically obtain β' values of ca. 900–1000 $\times 10^{-30}$ esu based on an 820 nm incident wavelength. For core–shell particles featuring silver mole fractions of 0.25, 0.50, and 0.57, respectively, we obtained β' values of 700, 600, and 1400 $\times 10^{-30}$ esu. These values are consistent with substantial plasmon enhancement. While it is somewhat surprising that the presence of a silver-like plasmon band near the two-photon wavelength does not lead to even larger β' values, theoretical studies of nanoparticle hyper-Rayleigh intensities [34] show that β' is most sensitive to the electromagnetic field intensity at the particle surface. This intensity does not have the same wavelength dependence as extinction, nor the same dependence on particle size [35].

4. Conclusions

Gold-core/silver-shell nanoparticles with 13 and 25 nm diameter cores and a range of shell thicknesses have been prepared by aqueous citrate reduction of silver nitrate in the presence of gold 'seed' nanoparticles. These particles, in contrast to alloy particles, display two distinct plasmon absorption bands and their relative intensities depend on the shell thickness – features that are captured well by the theory. While the observed bands resemble those seen with pure silver and pure gold nanospheres, the core/shell spectra are not simply linear combinations of the pure-component spectra. Theory shows that shell dielectric effects upon the core and vice versa, influence the extinction spectra, causing broadening, shifting, and, in some cases, damping of dominant spectral features. Finally, the core/shell particles show reasonably intense hyper-Rayleigh scattering under conditions of two-photon resonance or near resonance with a high-energy plasmon band.

References

[1] R.P. Andres, T. Bein, M. Dorogi, S. Feng, J.I. Henderson, C.P. Kubiak, W. Mahoney, R.G. Osifchin, R. Reifenberger, Science 272 (1996) 1323.

[2] R. Elghanian, J.J. Storhoff, R.C. Mucic, R.L. Letsinger, C.A. Mirkin, Science 277 (1997) 1078.

[3] G. Schmid, Adv. Mater. 10 (1998) 515.

[4] W.P. Mcconnell, J.P. Novak, L.C. Brousseau III, R.R. Fuierer, R.C. Tenent, D.L. Feldheim, J. Phys. Chem. B 104 (2000) 8925.

[5] S.H. Kim, G. Medeiros-Ribeiro, D.A.A. Ohlberg, R.S. Williams, J.R. Heath, J. Phys. Chem. B 103 (1999) 10341.

[6] T. Ung, L.M. Liz-Marzan, P. Mulvaney, J. Phys. Chem. B 103 (1999) 6770.

[7] J.J. Pietron, J.F. Hicks, R.W. Murray, J. Am. Chem. Soc. 121 (1999) 5565.

[8] K. Clays, E. Hendrickx, M. Triest, A. Persoons, J. Mol. Liq. 67 (1995) 133.

[9] M. Brust, M. Walker, D. Bethell, D.J. Schiffrin, R. Whyman, Chem. Commun. (1994) 801.

[10] L. He, M.D. Musick, S.R. Nicewarner, F.G. Salinas, S.J. Benkovic, M.J. Natan, C.D. Keating, J. Am. Chem. Soc. 122 (2000) 9071.

[11] For an overview, see: U. Kreibig, M. Vollmer, in: Optical Properties of Metal Clusters, Springer Series in Materials Science, vol. 25, Springer, Berlin, 1995, p. 187.

[12] Brandt, T.M. Cotton, Investigations of Surfaces and Interfaces, second ed., Wiley, New York, 1993.

[13] R.G. Freeman, K.C. Grabar, K.J. Allison, R.M. Bright, J.A. Davis, A.P. Guthrie, M.B. Hommer, M.A. Jackson, P.C. Smith, D.G. Walter, M.J. Natan, Science 267 (1995) 1629.

[14] S.J. Oldenburg, S.L. Westcott, R.D. Averitt, N.J. Halas, J. Chem. Phys. 111 (1999) 4729.

[15] I. Srnova-Sloufova, B. Vlckova, T.L. Snoeck, D.J. Stufkens, P. Matejka, Inorg. Chem. 39 (2000) 3551.

[16] P. Galletto, P.F. Brevet, H.H. Girault, R. Antoine, M. Broyer, J. Phys. Chem. B 103 (1999) 8706.

[17] F.W. Vance, B.I. Lemon, J.T. Hupp, J. Phys. Chem. B 102 (1998) 10091.

[18] J.P. Novak, L.C. Brousseau, F.W. Vance, R.C. Johnson, B.I. Lemon, J.T. Hupp, D.L. Feldheim, J. Am. Chem. Soc. 122 (2000) 12029.

[19] R.C. Johnson, J.T. Hupp, in: D.L. Feldheim, C. Foss (Eds.), Metal Nanoparticles: Synthesis Characterization and Applications, Marcel Dekker, New York, 2001.

[20] Y. Kim, R.C. Johnson, J.T. Hupp, Nano Lett. 1 (2001) 165.

[21] A. Henglein, P. Mulvaney, T. Linnert, A. Holzwarth, J. Phys. Chem. 96 (1992) 2411.

[22] P. Mulvaney, M. Giersig, A. Henglein, J. Phys. Chem. 96 (1992) 10419.

[23] A. Henglein, J. Phys. Chem. B 104 (2000) 2201.

[24] P. Mulvaney, M. Giersig, A. Henglein, J. Phys. Chem. 97 (1993) 7061.

[25] J. Sinzig, U. Radtke, M. Quinten, U. Kreibig, Z. Phys. D 26 (1993) 242.

[26] S. Link, Z.L. Wang, M.A. El-Sayed, J. Phys. Chem. B 103 (1999) 3529.

[27] G. Mie, Ann. Phys. 25 (1908) 377.

[28] C.F. Bohren, D.R. Huffman, Absorption and Scattering of Light by Small Particles, Wiley, New York, 1983.

[29] K.C. Grabar, R.G. Greeman, M.B. Hommer, M.J. Natan, Anal. Chem. 67 (1995) 735.

[30] J. Turkevich, P.C. Stevenson, J. Hillier, Discuss. Faraday Soc. 11 (1951) 55.

[31] A. Henglein, M. Giersig, J. Phys. Chem. B 103 (1999) 9533.

[32] E.W. Palik, Handbook of Optical Constants of Solids, Academic Press, New York, 1985.

[33] W.A. Kraus, G.C. Schatz, Chem. Phys. Lett. 99 (1983) 353.

[34] G.S. Agarwal, S.S. Jha, Solid State Commun. 41 (1982) 4999.

[35] K.L. Kelly, T.R. Jensen, A.A. Lazarides, G.C. Schatz, in: D.L. Feldheim, C. Foss (Eds.), Metal Nanoparticles: Synthesis, Characterization, and Applications, Marcel Dekker, New York, 2001.